Characterization of Wood Chars Produced at Different Temperatures Using Advanced Solid-State C-13 NMR Spectroscopic Techniques

ARTICLE *in* ENERGY & FUELS · SEPTEMBER 2012

Impact Factor: 2.79 · DOI: 10.1021/ef300947s

8 AUTHORS, INCLUDING:

Xiaoyan Cao
Brandeis University
33 PUBLICATIONS **313** CITATIONS
SEE PROFILE

Jingdong Mao
Old Dominion University
126 PUBLICATIONS **2,558** CITATIONS
SEE PROFILE

energy&fuels

Article

pubs.acs.org/EF

Characterization of Wood Chars Produced at Different Temperatures Using Advanced Solid-State ^{13}C NMR Spectroscopic Techniques

Xiaoyan Cao,[†] Joseph J. Pignatello,[‡] Yuan Li,[†] Charisma Lattao,[‡] Mark A. Chappell,[§] Na Chen,[†] Lesley F. Miller,[§] and Jingdong Mao*,[†]

[†]Department of Chemistry and Biochemistry, Old Dominion University, 4541 Hampton Boulevard, Norfolk, Virginia 23529, United States

[‡]Department of Environmental Sciences, The Connecticut Agricultural Experiment Station, Post Office Box 1106, New Haven, Connecticut 06504, United States

[§]Environmental Laboratory, United States Army Corps of Engineers, 3909 Halls Ferry Road, Vicksburg, Mississippi 39180, United States

ABSTRACT: Temperature is one of the controlling factors determining the chemical structure of char. We employed advanced solid-state ^{13}C NMR techniques to characterize maple wood and its chars produced under N_2 at temperatures from 300 to 700 °C. Our results indicated that 300 °C char was primarily composed of residues of biopolymers such as lignin and cellulose. Carbohydrates are completely lost for char prepared at 350 °C. At 400 °C, the char lost most of the ligno-cellulosic features and consisted predominantly of aromatic structures. By 500 °C, sp^3-hybridized carbon had all but disappeared. Protonated aromatic carbons increased up to 400 °C chars but then decreased. Aromatic C−O groups decreased, whereas nonprotonated aromatic carbons, especially bridgehead carbons, increased as temperature increased. The minimum aromatic cluster sizes estimated from spectral analysis increased from 8 carbons in 300 °C char, to 20, 18, 40, 64, and 76 carbons, respectively, in 350 °C, 400 °C, 500 °C, 600 °C, and 700 °C chars. $^1H-^{13}C$ long-range dipolar dephasing displayed the same increasing trend of aromatic cluster sizes of wood chars with increasing temperature. We show for the first time quantitative changes of different aromatic C forms and aromatic cluster size as a function of heat treatment temperature.

1. INTRODUCTION

Char is the carbonaceous material that remains after pyrolysis or incomplete burning of organic matter. As part of the black carbon continuum, chars are a ubiquitous component of soils and sediments, and their concentrations depend on the frequency of fires or the magnitude of intentional inputs of produced char. Wood chars have been manufactured for millennia. In addition to their traditional use as fuel, they have currently attracted attention as a means to improve soil fertility,[1−3] stabilize contaminated soil,[4,5] and offset greenhouse gas emissions,[6] among other applications. The physical and chemical properties of chars closely depend on feedstock types and processing variables such as temperature, duration of heating, oxygen availability, moisture content, mineral content, and how efficiently tarry volatiles are swept away.

Temperature is a critical parameter in char production. It is well recognized that with increasing heat treatment temperature (HTT) char yields and volatile carbon content decrease, while fixed carbon content and heating values increase.[7−11] The HTT affects the chemical composition of char[3,11] in ways important for their use. An understanding of the chemical structural variations of chars as a function of temperature is a prerequisite to successful tailoring of chars for specific purposes, and a comprehensive understanding of the natural charring process, which occurs under temperature gradient.[12]

An indispensable tool for characterizing chars is solid-state ^{13}C NMR spectroscopy. This technique, which reveals structural information at the molecular level nondestructively, has been used to determine structural changes of wood chars as a function of HTT.[12−15] Most studies to date have employed the ^{13}C cross-polarization magic angle spinning (CP/MAS) technique. The CP technique, however, does not provide reliable quantification of condensed aromatic carbons for two reasons: (i) CP of ^{13}C nuclei remote from protons is inefficient, and (ii) chars contain a high concentration of stabilized free radicals, which decrease proton rotating-frame spin−lattice relaxation time ($T_{1\rho}H$) and reduce the efficiency of magnetization transfer. The ^{13}C NMR direct polarization (DP) technique more accurately quantifies the structure of chars.

The degree of aromatic ring condensation is an important feature of char structure. Fused ring size generally increases with thermal alteration, tending toward the graphite structure.[16] Until recently, there had been no widely accepted method, however, for evaluating the degree of aromatic condensation in chars.[15,17−19] In a wet chemical approach, chars are partially oxidized with nitric acid into single-ring aromatic molecules with multiple carboxylic acid groups (benzene polycarboxylic acids or BPCAs), and a qualitative assessment of aromatic cluster size can be inferred from the distribution of individual BPCA molecular markers.[20−24] Basically, aromatic rings at the edges of the char structure tend to yield more of the lesser carboxylated BPCAs, whereas core aromatic rings in the char are more likely to form more of the greater carboxylated BPCAs.[21,25−27] The condensation degree of aromatic structures has also been explored using NMR methodology. Attempts

Received: June 1, 2012
Published: August 9, 2012

   dx.doi.org/10.1021/ef300947s | *Energy Fuels* 2012, 26, 5983−5991

based on the quantification of bridgehead carbon (aromatic carbons shared by two or more aromatic rings) by the simple CP/MAS or DP/MAS technique are plausible[28] but most likely to fail because spectral separation of bridgehead C from other nonprotonated aromatic C cannot be achieved, as detailed in Brewer et al.[18] and Mao et al.[29] Smernik and McBeath et al.[17,19,30] introduced a method that involves adding ^{13}C-labeled benzene to char and observing the changes in ^{13}C chemical shift experienced by benzene when sorbed to the char. The principle is that conjugated aromatic structures in chars in the presence of magnetic field induce diamagnetic ring currents, which cause the displacement of ^{13}C chemical shift of ^{13}C-labeled benzene sorbed to the char. The magnitude of this shift is shown to depend on the degree of aromatic condensation.[17] Brewer et al.[18] proposed a NMR-based protocol to estimate aromatic cluster size of chars involving long-range ^{1}H−^{13}C dipolar dephasing[31] and spectral analysis. This dual NMR approach has proven consistent and reliable for this purpose.

In the present study, we employed advanced solid-state ^{13}C NMR techniques such as quantitative DP/MAS in combination with dipolar dephasing, and ^{13}C chemical shift anisotropy filter to characterize the structures of maple wood and its chars produced at HTT from 300 to 700 °C. The size of fused aromatic rings was evaluated using the dual NMR methodology.[18,29] Brewer et al.[18] used the techniques to compare slow pyrolysis, fast pyrolysis, and gasification charring processes applied to different herbaceous feedstocks. We apply the techniques here to explore how structural changes of wood from a single source vary systematically with HTT during slow pyrolysis. We show the quantitative changes of different aromatic C forms (aromatic C−H, aromatic C−C, aromatic C−O, aromatic edge C, or bridgehead C) and aromatic cluster sizes, and provide detailed structures of wood chars with increasing HTT. The present study also aims to compare aromatic cluster sizes derived from dual NMR approach with the published results from ring current measurements.[19]

2. EXPERIMENTAL SECTION

2.1. Pyrolysis Procedure. Maple wood shavings were packed into a stainless steel reactor placed in the center zone of a temperature-programmable three-zone tube furnace (Lindburg Blue M Tube Furnace; Asheville, NC, U.S.A.). In a flow of N_2 (1.5 L/min), the shavings were heated at 100 °C for 1 h to drive off moisture and then heated at the rate of 25 °C/min to the desired HTT and held for 2 h. The HTT was varied from 300 to 700 °C. The chars were stored for at least 2 weeks in air to complete chemisorption of oxygen and then gently pulverized to pass a 100 mesh screen. Elemental analysis (C, H, N, O, and ash) was performed by Galbraith Laboratories, Inc. (Knoxville, TN) and the results are given in Table 1.

Table 1. Elemental Analysis of Maple Wood and Chars Prepared under Different Thermal Conditions

	% by weight					atomic ratio	
samples	C	H	O	N	ash	H/C	O/C
maple wood	53.4	6.8	39.8	<0.5	1.0	1.53	0.56
300 °C char	60.8	5.6	31.1	<0.5	0.8	1.11	0.38
350 °C char	72.5	4.6	21.7	<0.5	2.2	0.77	0.22
400 °C char	74.8	4.0	18.6	<0.5	1.7	0.64	0.19
500 °C char	83.2	3.2	10.6	<0.5	1.8	0.47	0.10
600 °C char	86.3	2.5	7.2	<0.5	2.2	0.35	0.06
700 °C char	84.4	1.9	6.7	<0.5	3.4	0.26	0.06

2.2. NMR Spectroscopy. ^{13}C NMR analyses were performed using a Bruker Avance III 300 spectrometer at 75 MHz (300 MHz ^{1}H frequency). All experiments were run in a double-resonance probe head using 4-mm sample rotors.

2.2.1. Quantitative ^{13}C DP/MAS and DP/MAS with Recoupled Dipolar Dephasing (DP/MAS/DD) NMR. Quantitative ^{13}C DP/MAS NMR experiments were performed at a spinning speed of 13 kHz. The 90° ^{13}C pulse length was 4 μs. Recycle delays, ranging from 10 to 40 s, were determined by the cross-polarization/spin−lattice relaxation time/total sideband suppression (CP/T_1-TOSS) technique to ensure all carbon nuclei were relaxed by more than 95%.[32] Nonprotonated carbons and mobile carbon fractions were quantified using a combination of DP/MAS technique and a recoupled dipolar-dephasing delay of 68 μs.[33] The recycle delays for DP/MAS and DP/MAS with dipolar dephasing were 40 s, 30 s, 40 s, 30 s, 40 s, 30 s, and 10 s, respectively, for maple wood, 300 °C, 350 °C, 400 °C, 500 °C, 600 °C, and 700 °C chars. For those not fully relaxed, the ^{13}C NMR spectra were corrected for incomplete relaxation by factors measured in CP/T_1-TOSS.[32] The number of scans for DP/MAS and DP/MAS/DD experiments for all samples was 1024.

2.2.2. ^{13}C Cross-Polarization and Total Suppression of Sidebands (CP/TOSS) and ^{13}C CP/TOSS Plus Dipolar Dephasing (CP/TOSS/DD). Semiquantitative compositional information was obtained with good sensitivity using a ^{13}C CP/MAS NMR technique with MAS 5 kHz, CP time 1 ms, and ^{1}H 90° pulse-length 4 μs. Four-pulse total suppression of sidebands (TOSS)[34] was employed before detection, with the two-pulse phase-modulated (TPPM) decoupling applied for optimum resolution. Subspectra for nonprotonated and mobile carbon groups were obtained by combining the ^{13}C CP/TOSS sequence with a 40-μs dipolar dephasing. The number of scans for ^{13}C CP/TOSS and ^{13}C CP/TOSS/DD experiments was 6144 for all samples.

2.2.3. ^{13}C Chemical-Shift-Anisotropy (CSA) Filter. Since O−C−O carbons (e.g., anomeric C in carbohydrate rings) and aromatic carbon resonances between 120 and 90 ppm are difficult to resolve, the aromatic carbon signals were selectively suppressed using a five-pulse ^{13}C CSA filter with a CSA-filter time of 47 μs.[35] The number of scans was 6144 for all samples.

2.2.4. Spectral Editing of Immobile CH_2 + CH. Spectra for immobile CH_2 + CH groups were obtained using the following spectral-editing techniques. First, a ^{13}C CP/TOSS spectrum was recorded using a short CP time (50 μs) to emphasize protonated carbons in immobile segments. Afterward, a second ^{13}C CP/TOSS spectrum was recorded using a short CP (50 μs) coupled with a 40 μs dipolar dephasing. The difference spectrum of the two represents immobile CH_2 and CH carbons, with a small CH_3 contribution.[36] The number of scans was 6144 for all samples.

2.2.5. ^{1}H−^{13}C Long-Range Recoupled Dipolar Dephasing Experiments. The size of fused aromatic rings was estimated from the recoupled ^{1}H−^{13}C dipolar dephasing.[31] In short, two ^{1}H 180° pulses per rotation period prevent MAS from averaging out weak CH dipolar couplings. To detect nonprotonated carbons with good relative efficiency, direct polarization/total sideband suppression (DP/TOSS) was used at a spinning rate of 7 kHz. The ^{13}C 90° and 180°-pulse lengths were 4 and 8 μs, respectively. The number of scans was 640 for all char samples at each dephasing time.

3. RESULTS AND DISCUSSION

3.1. Chemical Structural Changes of Chars with Increasing HTT. Elemental analysis of the samples (Table 1) shows loss of oxygen and hydrogen and enrichment of carbon with increasing HTT. The 700 °C char has slightly lower carbon content than the 600 °C char. The H/C and O/C atomic ratios decrease with HTT and correlate strongly with one another (R^2 = 0.99), most likely associated with dehydration and condensation reactions. The nitrogen contents are relatively low (<0.5%) for wood and wood chars, excluding the presence of significant amounts of N-containing com-

dx.doi.org/10.1021/ef300947s | Energy Fuels 2012, 26, 5983−5991

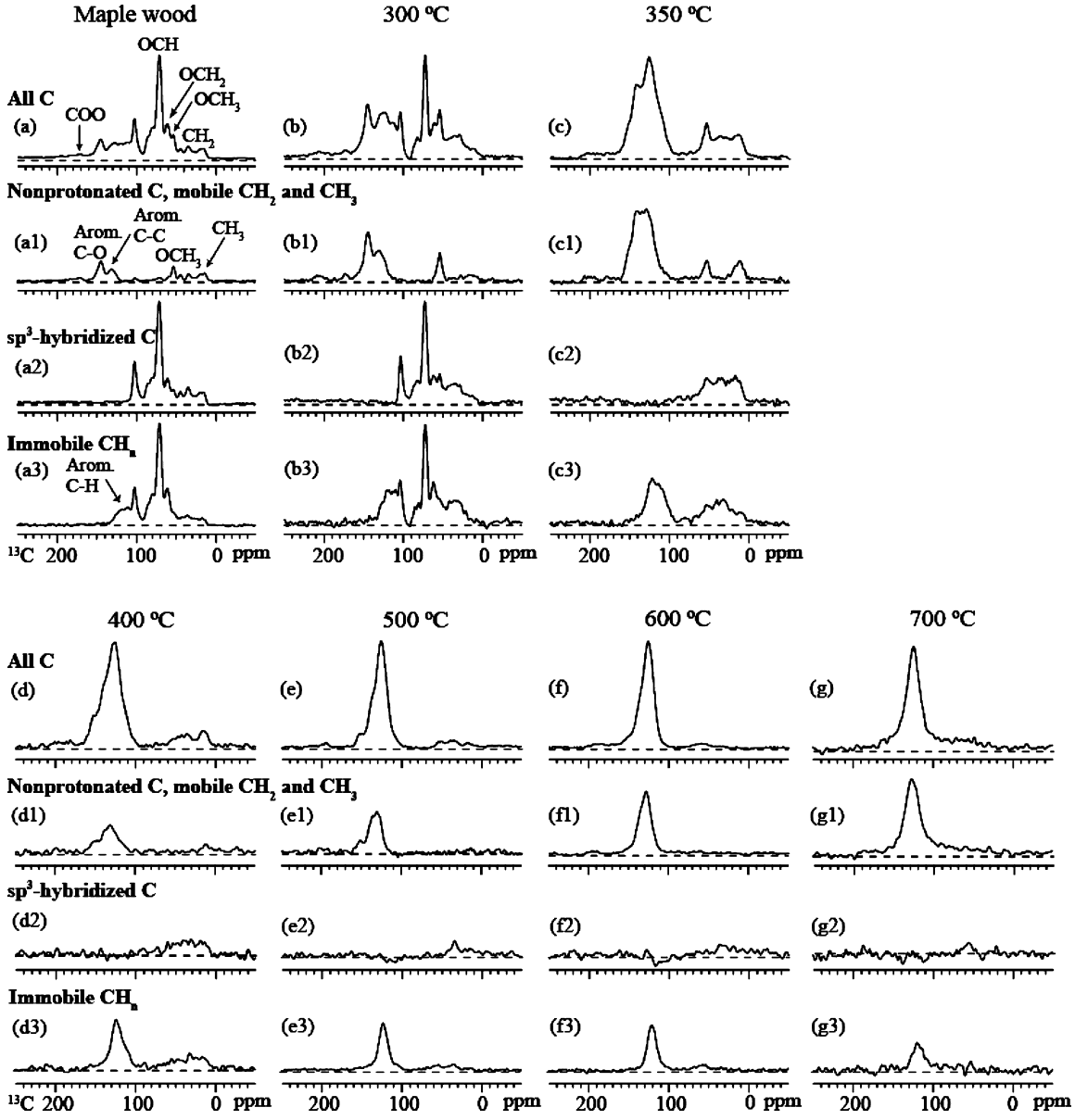

Figure 1. Spectral editing for identification of functional groups in maple wood and its chars. (a–g) Unselective CP/TOSS spectra for reference. (a1–g1) Corresponding dipolar-dephased CP/TOSS spectra show nonprotonated carbons and mobile segments such as CH_3. (a2–g2) Selection of sp^3-hybridized carbon signals by a ^{13}C CSA filter. (a3–g3) Selection of relatively immobile CH and CH_2 signals with small residual CH_3, achieved by the difference between a short-CP spectrum and a spectrum of short-CP combined with dipolar dephasing.

pounds. Ash content trends upward with temperature due to the depletion of residual organic material.

Figure 1 shows the spectra from ^{13}C CP/TOSS and spectral editing techniques of maple wood and its chars prepared at 300–700 °C. The use of CP gives a better signal-to-noise ratio in a shorter experimental time, and spectral editing techniques aid in assignment of overlapping resonances. All spectra are scaled to match the intensity of the highest band.

The top spectra (Figure 1a–g) are ^{13}C CP/TOSS spectra showing signals from all carbon sites. The spectrum of untreated maple wood (Figure 1a) is typical of spectra obtained for unaltered wood samples.[12,15,37,38] The signals from the following functional groups are observed: (1) alkyl carbons, with the signal at 18 ppm assigned to methyl (CH_3COO of hemicellulose), and 30 ppm to methylene carbons; (2) methoxyl carbons ($ArOCH_3$ of lignin), resonating around 45–62 ppm; (3) *O*-alkyl carbons including OCH_2 groups (C6 carbons of cellulose) at 62 ppm, OCH groups (C2, C3 and C5 carbons of cellulose or hemicellulose) exhibiting a sharp peak at 72 ppm, and OCH groups (C4 carbons of cellulose or C_β carbons of lignin) displaying a shoulder at 82 ppm; (4) di-*O*-alkyl carbons with a sharp peak at 103 ppm and the right shoulder overlapping with aromatic carbon resonances; (5) nonoxygenated aromatic carbons around 110–140 ppm; and (6) oxygenated aromatic carbons (148 ppm). There are also some weak signals near 173 ppm, attributable to COOR/CH_3COO groups. These identified signals are indicative of the presence of biopolymers such as lignin (57, 128, and 148 ppm) and cellulose or hemicellulose (62, 72, 82, and 103 ppm) in maple wood.

The spectrum of the 300 °C char (Figure 1b) retains most of the ligno-cellulosic features, as shown by the presence of characteristic peaks of lignin and cellulose/hemicellulose. Several spectral changes are noted in the spectrum of the 300

dx.doi.org/10.1021/ef300947s | *Energy Fuels* 2012, 26, 5983–5991

°C char: (1) broadening of alkyl carbon signals; (2) relative enrichment of signals arising from methylene, OCH_3, and aromatic carbons, as compared with signals from *O*-alkyl and di-*O*-alkyl carbons; and (3) the appearance of a small signal around 206 ppm assigned to ketone/aldehyde carbons.

Major spectral changes occur on increasing the HTT from 300 to 350 °C (Figure 1c). Signals of *O*-alkyl and di-*O*-alkyl carbons are completely depleted while the aromatic resonances become dominant. The oxygenated aromatic carbon peak (∼ 148 ppm) and methoxyl peak (∼ 57 ppm) are quite prominent and indicate the presence of altered lignin residues in 350 °C char. In the spectrum of the 400 °C char (Figure 1d) the lignocellulosic features[38] nearly disappear. The signals of methyl and methylene groups are markedly reduced in intensity. The oxygenated aromatic carbon peak (∼ 148 ppm) is decreased in intensity and becomes a shoulder (∼ 152 ppm) on the downfield side of the aromatic band. Above 400 °C, the ^{13}C NMR CP/TOSS spectra (Figure 1e−g) show further decrease in the peak intensities of alkyl carbons. In addition, intensity of oxygenated aromatic carbons at 152 ppm decreases, leading to narrowing of the aromatic bands. The spectrum of 600 °C char yields the best signal-to-noise ratio for aromatic band. The resonance line of aromatic carbons in the spectrum of the 700 °C char, however, becomes much broader, and may obscure any residual aliphatic signals if present. Solum et al.[15] and Freitas et al.[39,40] also reported similar findings in their studies of chars from different organic precursors (white oak chars, peat, rice hulls, and polyvinyl chloride), prepared at HTT of 550 °C and above. Both groups attributed the broadening to either an increase in conductivity of the sample, or the occurrence of a larger number of delocalized π electrons around the ^{13}C nuclei arising from the growth of the aromatic planes of the chars at higher HTT. Freitas et al.[40] excluded the presence of free radicals during pyrolysis as the cause for the increasing line width of the aromatic band by reasoning that the line width continued to increase with HTT above 700 °C, when concentrations of the radicals are supposed to decrease after passing through a maximum at HTT near 400−700 °C. Another explanation could be the presence of paramagnetic mineral impurities in the chars,[39] which increase with ash content as HTT rises (Table 1), but this is likely to be only a minor effect.

Spectra in the second row (Figure 1a1−g1) are CP/TOSS spectra obtained after dipolar dephasing, which highlight signals from nonprotonated carbons and mobile carbon groups. The dipolar-dephased spectrum of the maple wood (Figure 1a1) displays peaks from methyl carbons, mobile $(CH_2)_n$ carbons, methoxyl carbons, nonprotonated aromatic C−C carbons, aromatic C−O carbons, and COOR carbons. The strong suppression of the signal at ∼103 ppm after dipolar-dephasing indicates that di-*O*-alkyl carbons are all protonated anomeric carbons. In the dipolar-dephased spectrum of the 300 °C char (Figure 1b1), major peaks are observed from OCH_3 carbons, aromatic C−C carbons, and aromatic C−O carbons. The corresponding spectrum of the 350 °C char (Figure 1c1) shows signals primarily from aromatic C−C carbons and aromatic C−O carbons, as well as signals from OCH_3 and CCH_3 carbons in much lower abundance. The dipolar-dephased spectra of the 400−700 °C chars (Figure 1d1−g1) are dominated by signals from nonprotonated aromatic carbons. The intensity of the aromatic C−O shoulder at about 150 ppm progressively decreases with HTT, leading to a more symmetrical aromatic peak. We note the disappearance of signals associated with OCH_3 groups (∼57 ppm) in spectra of chars prepared at 400 °C and above: the absence of this peak indicates that other aromatic C−O groups such as phenolic −OH, rather than aromatic C-OCH_3, account for the signals around 150 ppm. The char at 400 °C displays weak signals from methyl carbons that are absent in the chars at higher HTT.

Figure 1a2−g2 exhibits CP/TOSS spectra after the insertion of the CSA filter, which selects for resonances of sp^3-hybridized carbons. The spectra of maple wood and the 300 °C char (Figure 1a2−b2) show a well-defined aliphatic region, and more importantly, the signal from di-*O*-alkyl is clearly separated from overlapping aromatic carbon signals. Signals of *O*-alkyl and di-*O*-alkyl carbons are clearly absent in spectra of chars prepared at 350 °C and above. The spectra of other chars display only broad alkyl bands with intensities that decrease with increasing HTT.

Figure 1a3−g3 exhibits spectra selecting for relatively immobile CH and CH_2 signals with small residual CH_3. The spectra of maple wood and the 300 °C char (Figure 1a3−b3) show a well-defined aliphatic region that resembles those in the respective CP/TOSS spectrum. In the aromatic region, the protonated aromatic signals at ∼120 ppm overlap with di-*O*-alkyl signals at ∼103 ppm. From 350 °C upward, the immobile CH_n spectra (Figure 1c3−g3) are dominated mainly by resonances of protonated aromatic carbons; intensities of signals from aliphatic CCH and CCH_2C carbons are relatively lower and decrease with increasing HTT. The protonated aromatic peaks are more symmetrical and appear upfield of their corresponding nonprotonated aromatic peaks.

Quantitative chemical composition of chars can be more reliably obtained from DP spectra. Figure 2 presents the spectra of ^{13}C DP/MAS (thin lines) and ^{13}C DP/MAS with 68-μs recoupled dipolar dephasing (thick lines) of all samples. The former permits quantitative structural information of all carbons and the latter of nonprotonated and mobile carbons. The DP and DP/DD spectra show similar general features as the CP spectra. Nevertheless, signals from aromatic carbons are clearly underestimated in CP spectra relative to their corresponding DP spectra of chars. The relative percentages of different functional groups obtained from DP and DP/DD spectra are compiled in Table 2. Compared to unaltered wood sample, composition of 300 °C char shows the depletion of alkyl and *O*-alkyl carbons, the accumulation of aromatic carbons including protonated, nonprotonated, and oxygenated aromatic carbons, as well as a slight increase of COOR and ketone/aldehyde carbons. Carbohydrates are completely lost for chars of 350 °C and above. In addition, abundances of non-oxygenated aromatic carbons prominently increase while those of oxygenated aromatic carbons decrease in the 350 °C char. Abundances of alkyl carbons and O-containing functional groups (*O*-alkyl, aromatic C−O groups, COOR, and ketone/aldehyde) generally decrease as HTT further increases. The 700 °C char contains an anomalously high signal around 45−90 ppm usually assigned to alkyls and *O*-alkyls. As the elemental analysis shows a consistent trend of loss of oxygen with HTT, the intensities observed cannot be attributed to oxygen functional groups but to the broadening of the aromatic band extending from ∼45 to ∼200 ppm in its CP and DP spectra (Figures 1g and 2g).

An important advantage of DP is that it more reliably estimates total aromaticity and nonprotonated aromaticity. The fraction of total aromatic carbon (F_{aro}) is defined as the sum of the fractions of protonated aromatic carbon (F_{Haro}; C−H),

dx.doi.org/10.1021/ef300947s | *Energy Fuels* 2012, 26, 5983−5991

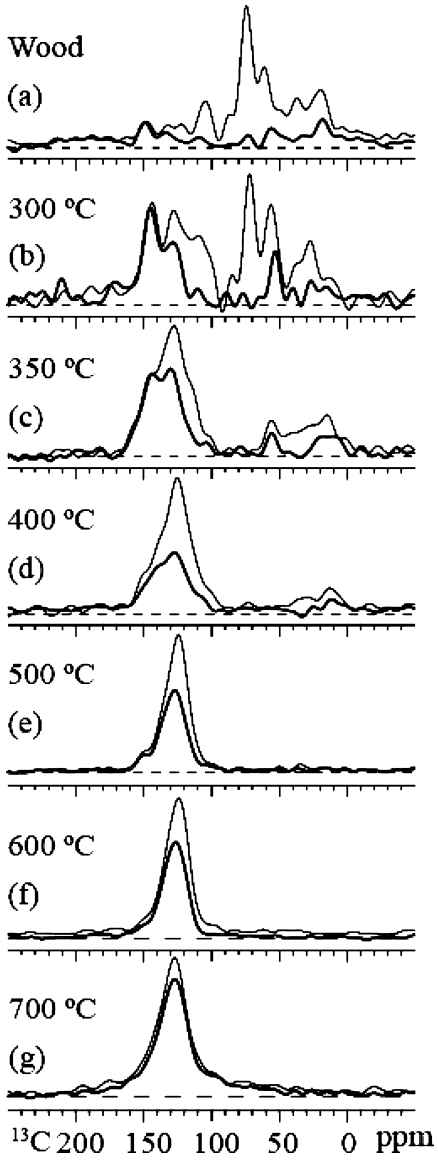

Figure 2. Quantitative ^{13}C DP/MAS NMR spectra (thin lines) and DP/MAS after recoupled dipolar dephasing showing nonprotonated carbons plus mobile groups such as CH_3 (thick lines). Spectra are scaled to match the intensity of the highest band.

nonprotonated aromatic (F_{naro}; C−C), and oxygenated aromatic carbon (F_{Oaro}; C−O) relative to total carbon. Nonprotonated aromatic carbons are, further, a mixture of edge and bridgehead aromatic carbons. The F_{aro} reaches a maximum at 600 °C (Table 3). The slight decrease of F_{aro} in the 700 °C char may be due to broadening of the aromatic band, part of which is integrated as "oxygen-containing" functional groups. Similar observations were reported for a char made from chlorogenic acid at 650 °C.[41] The F_{naro} generally increases with increasing HTT. As potential C-substituents (alkyls and carbonyl groups) decrease with increasing HTT, the fraction of C-substituted edge aromatic carbons can be expected to decrease. Therefore, the increase of F_{naro} may be exclusively attributed to the increase of bridgehead aromatic carbons with increasing HTT. The F_{Haro} increases from 4.0% in unaltered wood, to 12.8%, 25.2%, and 37.8% in 300 °C, 350 and 400 °C chars, respectively. Czimczik et al.[12] also reported an increase of F_{Haro} upon increasing the HTT of wood chars from 350 to 480 °C. However, in the present study, charring above 400 °C results in a decrease in F_{Haro}. In particular, the ratio F_{naro}/F_{Haro} increases from 0.5 for unaltered wood, to ∼1.0 for the 300 °C, 350 °C, and 400 °C chars, and then to 2.0, 3.0, and 9.0 for the 500 °C, 600 °C, and 700 °C chars, respectively. The ratio is highest for the 700 °C char, despite its relatively lower F_{aro}. Considering the negligible alkyl signal in 500−700 °C chars, it is reasonable to believe that the increase in the F_{naro}/F_{Haro} ratio arises from the condensation of aromatic rings.

3.2. Estimation of Aromatic Cluster Size from Spectral Analysis and Long-Range ^{1}H−^{13}C Dipolar Dephasing.

Aromatic cluster size, as a measure of the degree of aromatic condensation, can be estimated by combining two complementary NMR approaches: spectral analysis[18,29] and recoupled long-range ^{1}H−^{13}C dipolar dephasing.[31] The former arrives at the aromatic cluster size by estimating the fraction of carbons along the edges of the aromatic rings (χ_{edge}). Details of the calculations are given by Brewer et al.[18] The minimum and maximum aromatic edge fractions ($\chi_{edge,\ min}$ and $\chi_{edge,\ max}$) listed in Table 3 show quite limited ranges, especially for the 350 °C, 400 °C, 500 °C, and 600 °C chars. Estimation of χ_{edge} allows assessment of condensation geometry (linear versus circular catenation). Polycyclic aromatic hydrocarbons (PAHs) with linear catenation belong to the $C_{4n+2}H_{2n+4}$ family and therefore have $\chi_{edge} > 0.5$.[28] Applying this rationale to the chars of the

Table 2. Composition of Functional Groups (%) in Maple Wood and Chars Obtained by Quantitative DP/NMR Analyses[a]

	ppm								
	220−184	184−165	165−146	146−90		110−90	90−45	45−20	20−0
samples	aldehyde/ketone	COOR	arom. C−O	nonproton. arom. C−C	proton. arom. C−H	di-*O*-alkyl	*O*-alkyl	CH_2	CH_3
maple wood	0.0	0.0	3.7	2.2	4.0	8.0	54.6	18.4	9.2
300 °C char	2.7	2.5	16.9	11.2	12.8	7.5	31.1	11.6	3.6
350 °C char	1.2	1.0	11.7	34.2	25.2	0.0	8.5	9.8	8.3
400 °C char	0.3	1.5	8.1	37.4	37.8	0.0	3.3	5.1	6.5
500 °C char	0.7	1.0	5.8	58.6	28.9	0.0	1.7	2.2	1.2
600 °C char	0.0	1.7	4.5	68.0	23.0	0.0	2.1	0.7	0.0
700 °C char	2.5	4.1	9.2	65.7	7.3	0.0	8.0	2.3	1.1

[a]Sidebands are corrected and added to the centerband based on methods provided by Mao and Schmidt-Rohr.[33] The percentages in each row add up to 100. Note that for maple wood and 300 °C char, the spectral range of 110−137 ppm is assigned to aromatic C−C and aromatic C−H carbons, and that of 137−165 ppm is assigned to aromatic C−O groups. For other wood char samples, the signals from anomeric di-*O*-alkyl carbons are absent from the subspectra (Figure 1c2−g2) obtained by ^{13}C CSA filter, and thus aromatic carbons are acquired by integrating the spectral range 90−146 ppm.

dx.doi.org/10.1021/ef300947s | *Energy Fuels* 2012, 26, 5983−5991

Table 3. Structural Parameters Derived from Quantitative ^{13}C DP/MAS Spectra

samples	F_{aro}[a] (%)	F_{alkyl}[b] (%)	F_{Oaro} (%)	F_{naro} (%)	F_{Haro} (%)	F_{naro}/F_{Haro}	F_{Haro}/F_{aro}	$\chi_{edge,\ min}$[c]	$\chi_{edge,\ max}$[d]
maple wood	9.8	90.2	3.7	2.2	4.0	0.5	0.40	NA	NA
300 °C char	41.0	53.9	16.9	11.2	12.8	0.9	0.31	0.73	0.85
350 °C char	71.1	26.6	11.7	34.2	25.2	1.4	0.35	0.52	0.55
400 °C char	83.3	14.8	8.1	37.4	37.8	1.0	0.45	0.55	0.57
500 °C char	93.3	5.1	5.8	58.6	28.9	2.0	0.31	0.37	0.39
600 °C char	95.5	2.8	4.5	68.0	23.0	3.0	0.24	0.29	0.31
700 °C char	82.1	11.3	9.2	65.7	7.3	9.0	0.09	0.20	0.28

[a] F_{aro} (165−110 ppm) = F_{Oaro} + F_{naro} + F_{Haro}. [b] F_{alkyl} (110−0 ppm). [c] $\chi_{edge,\ min} = (F_{Haro} + F_{Oaro})/F_{aro}$. [d] $\chi_{edge,\ max} = \chi_{edge,\ min} + (F_{alkyl} + F_{C=O} + F_{COO})/F_{aro}$.

present study, we conclude that linear catenation of aromatic structures in the 500 °C, 600 °C, and 700 °C chars can be ruled out because $\chi_{edge} < 0.5$. The 300 °C, 350 °C, and 400 °C chars having $\chi_{edge} > 0.5$ are less condensed but not necessarily linearly catenated. We realize that all chars in the present study may contain some oxygen-containing and alkyl substituents to the aromatic rings. Hence, the rationale of Solum et al.[28] based on PAHs provide only a rough picture of the geometry of condensation of the chars in the present study. As HTT increases, χ_{edge} decreases, resulting in an increase in the fraction of bridgehead carbons χ_{bridge}. The average aromatic cluster size can be obtained using the equations in Solum et al.:[18,28] upper limit for linear catenation, $n_{C,\ max} \leq 3/(\chi_{edge} - 0.5) \leq 3/(\chi_{edge,\ min} - 0.5)$; lower limit for circular catenation, $n_{C,\ min} \geq 6/\chi_{edge}^2 \geq 6/\chi_{edge,\ max}^2$.

The minimum average cluster size of chars versus HTT is shown in Figure 3. The 300 °C char has an average of more

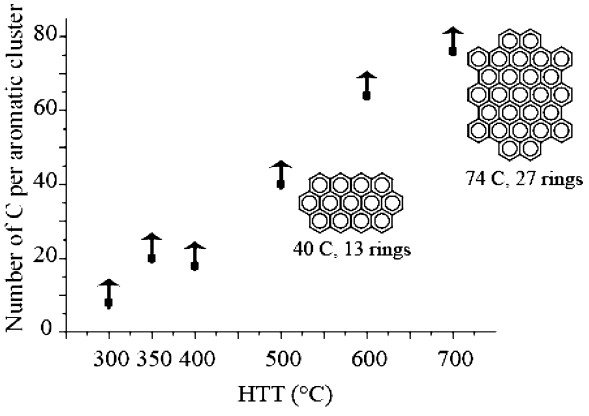

Figure 3. Plot of the minimum average cluster size of chars versus HTT.

than 8 carbons (circular catenation), or less than 13 carbons (linear catenation), in its average aromatic cluster. Thus, 1−2 aromatic rings can be expected. The 350 and 400 °C chars have minimum aromatic cluster sizes of 20 and 18 carbons (circular catenation), respectively. In general, chars formed at relatively low HTT (<500 °C) consist mainly of small clusters of condensed carbons, and lack a high proportion of bridgehead C. The aromatic cluster sizes of chars increase substantially with further increase in HTT, having more than 40, 64, and 76 carbons in the aromatic clusters of the 500 °C, 600 °C, and 700 °C chars, respectively. The geometry of aromatic condensation in these chars follows the circular catenation.[18,28,29] Examples of hypothetical circularly catenated ring systems containing 74 and 40 carbons are shown in Figure 3.

The second approach, long-range $^1H-^{13}C$ dipolar dephasing, probes the variation in distance of a carbon from the nearest proton and thus gives information on aromatic cluster size. This is achieved by comparing the dephasing rates of aromatic carbons. The slower the dephasing of the aromatic carbon signal, the longer the average $^1H-^{13}C$ interatomic distance, and thus the larger the average aromatic cluster size. Figure 4 shows

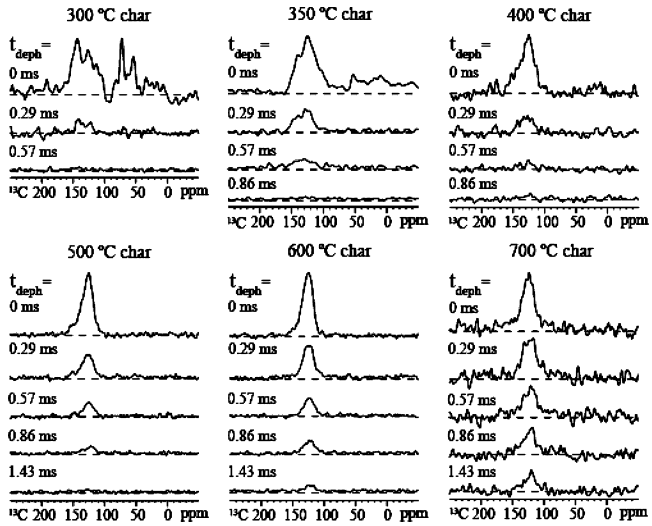

Figure 4. Series of ^{13}C DP/TOSS spectra after $^1H-^{13}C$ recoupled long-range dipolar dephasing of the indicated durations t_{deph} of 300 °C, 350 °C, 400 °C, 500 °C, 600 °C, and 700 °C chars.

the loss of aromatic signals in the DP/TOSS spectra with the dephasing time. The aromatic signals of the 300 °C char almost disappear after a dephasing time as short as 0.57 ms, whereas those of the 600 °C and 700 °C chars are still present even at 1.43 ms. Figure 5 displays the dephasing rate curves of the aromatic carbons of the six chars as well as two model compounds (3-methoxy benzamide, and 1,8-dihydroxy-3-methylanthraquinone).[31] The dephasing rate of the chars decreases with HTT, consistent with increasing aromatic cluster size as determined by spectral analysis. The curves for specific sites in model compounds C-1 of 3-methoxy benzamide and C-11 of 1,8-dihydroxy-3-methylanthraquinone (dashed lines in Figure 5), with two two-bond and two three-bond couplings, respectively, provide an approximate length-scale calibration. The dephasing rate of the 300 °C char nearly coincides with that of the two-bond model, indicating that the carbons in this char are on average at a two-bond distance from the nearest proton. Brewer et al.[18] found coincidence of the two-bond dephasing calibration curve with that of the milled-wood lignin. Therefore, 300 °C char in the present study has a similar average aromatic ring size as the milled-wood lignin. The

dx.doi.org/10.1021/ef300947s | Energy Fuels 2012, 26, 5983−5991

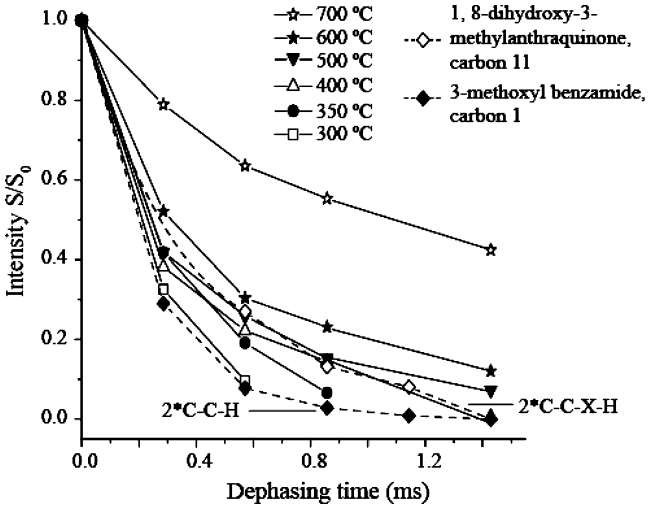

Figure 5. Plot of the area of signals of aromatic carbons resonating between 107 and 142 ppm versus dephasing time. Open stars: 700 °C char. Solid stars: 600 °C char. Solid triangles: 500 °C char. Open triangles: 400 °C char. Solid circles: 350 °C char. Open squares: 300 °C char. Open diamonds: Carbon 11 of 1,8-dihydroxy-3-methylanthraquinone, which is three bonds away from the three nearest protons. Solid diamonds: Carbon 1 of 3-methoxy benzamide, which is two bonds away from the two nearest protons. Data have been corrected for regular T_2 relaxation.

dephasing rate of 350 °C char is apparently slower than that of the 300 °C char, but it is comparable to that of 400 °C char. The 500 °C char has a slightly slower dephasing rate compared to the 400 °C char, but both dephasing curves are similar to that of the three-bond calibration curve. The dephasing rate of 600 °C char is slower than that of C-11 of 1,8-dihydroxy-3-methylanthraquinone, indicating that carbons in this char are relatively more than three bonds away from a couple of protons, on average. The slowest dephasing rate is observed for the 700 °C char, which requires a significantly larger fraction of C at a larger than three-bond distance from the nearest proton.

Estimations of aromatic cluster size for chars derived from the two NMR approaches used are consistent. The 300 °C HTT produces a material with small cluster size of 1−2 aromatic rings, indicative of an aromatic structure derived from lignin that has only been slightly thermally altered. Condensation degree increases in 350 and 400 °C chars with more than 18 carbons in the aromatic cluster, with either linear or circular catenation possible.[28] In the 500−700 °C chars, aromatic clusters are more condensed and of the circular catenation type.[28] The positive correlation between temperature and aromatic cluster size[15,17,18] is hence corroborated by the dual NMR approach.

3.3. Comparison with Previous NMR Studies of Char.

Our results provide detailed structural changes of wood chars with increasing HTT based on advanced solid-state NMR methods that go beyond what has been presented previously on char structural changes with HTT. In agreement with previous NMR studies,[12,13,19,37,39,42,43] char becomes relatively enriched in aromatic carbon, and relatively depleted in all the nonaromatic carbons with increasing temperature. Whereas the cellulose signature is quite pronounced in the structure of the 300 °C char in the present study, some literature indicated that carbohydrates were markedly reduced in relative intensity for wood chars prepared at 300 °C or even at 250 °C.[19,43] These differences are most likely explained by different heating time and the presence/absence of additives (i.e., NaOH) during pyrolysis in those studies. Our results further identify 350−400 °C as the temperature range where ligno-cellulosic features of wood are lost during pyrolysis. According to McBeath et al.,[19] wood char aromaticity increases rapidly through the low temperature range 250−450 °C, exceeding 89% at a HTT of 400 °C. At HTT above 400 °C, aromaticity derived from their DP spectra was reported to be 99−100%. The same trend of increasing aromaticity with HTT is also observed in the present study for chars prepared from 300 to 700 °C, though the exact values are generally lower than those reported in McBeath et al.[19] The discrepancy is likely due to the difference in pyrolysis conditions (heating rate, heat treatment time, gas flow rate, etc.). In addition, the severe spinning sidebands present in their spectra may also have introduced uncertainty in the estimation of aromaticity. Solid-state ^{13}C NMR using the techniques of DP/MAS and DP/MAS with dipolar dephasing presented here further quantitatively characterize the evolution of aromatic C (aromatic C−H, aromatic C−C, aromatic C−O, aromatic edge C, or bridgehead C) with temperature, a result that has not been achieved in previous studies of wood chars. We find a decrease in aromatic C−O and edge C, but an increase in aromatic C−C (bridgehead C, in particular) as HTT increases. The abundance of aromatic C−H reaches a maximum at 400 °C but then decreases with higher HTT.

The degree of aromatic condensation is an important property of charred biomass. McBeath et al.[19] obtained a rough idea of aromatic condensation of chestnut wood chars produced from 200 to 1000 °C by measuring the chemical shift of sorbed ^{13}C-benzene (generally upfield relative to dissolved benzene) in comparison with the *ab initio* calculated ring-current shift of benzene situated parallel-planar over the centers of PAH molecules of different ring cluster size. They concluded that chars produced below 500 °C have no greater degree of condensation than coronene (i.e., seven fused aromatic rings), while those produced between 500 and 700 °C contain aromatic domains no larger than the 13 ring PAH hexabenzylcoronene, and chars produced above 700 °C are abundant in domains larger than 19 rings. Calculated shifts depend strongly on distance from, position over, and shape of the charring cluster. This approach ignores that these factors may themselves vary with HTT. It may ignore any contribution from sorption in anti-parallel conformations. Consistent with the McBeath study,[19] estimates of aromatic cluster size through spectral analysis in our study indicate relatively smaller aromatic clusters in 300−400 °C chars, whereas in contrast to their findings, aromatic cluster size for chars prepared at 600−700 °C are estimated to be larger than 13 rings. Except that the 350 and 400 °C chars of our study have a similar degree of condensation, our results confirm the positive correlation between temperature and aromatic cluster size previously indicated in the McBeath et al.[19] and other studies.[15,17,18]

NMR studies have also revealed the spectral similarity of chars produced at HTT above 600 °C regardless of their starting materials.[14,15,19,39,41,44−46] The final product above 600 °C is almost completely aromatic, although carboxyl carbons have been observed in chars even at 750 °C.[47] Despite their spectral similarity at high HTT, chars produced from different starting materials may differ in their degree of aromatic condensation. For example, McBeath and Smernik[17] indicated that aromatic structures in the wood char are more condensed than in the grass char produced at the same HTT. Brewer et al.[18] estimated that fused aromatic cluster size of switchgrass

dx.doi.org/10.1021/ef300947s | Energy Fuels 2012, 26, 5983−5991

chars produced by slow pyrolysis at 500 °C to be >23 C. Applying the same NMR approach, we found that wood chars prepared at 500 °C had an aromatic cluster size of >40 C. This suggests that feedstock type has an effect on the degree of aromatic condensation of chars.

4. CONCLUSIONS

Maple wood and its chars produced under N_2 at temperatures from 300 to 700 °C were characterized by advanced solid-state ^{13}C NMR spectroscopy to provide insight into chemical structure as a function of heat treatment temperature. Solid-state ^{13}C NMR techniques presented here quantitatively tracked changes in carbon structure and degree of aromatic condensation with temperature.

1. Heat treatment at 300 °C resulted in a material that was composed primarily of residues of biopolymers such as lignin and cellulose. Carbohydrates were completely lost for char prepared at 350 °C. At 400 °C and above, the char lost ligno-cellulosic features and consisted predominantly of aromatic structures.
2. The aromatic character of chars increased with heat treatment temperature. Protonated aromatic carbons increased up to 400 °C chars but then decreased. Aromatic C−O groups decreased whereas nonprotonated aromatic carbons, especially bridgehead carbons increased with temperature.
3. The positive temperature−ring size relationship was corroborated by the NMR-based protocol in this study. The minimum aromatic cluster sizes estimated from spectral analysis increased from 8 carbons in 300 °C char, to 20, 18, 40, 64, and 76 carbons, respectively, in 350 °C, 400 °C, 500 °C, 600 °C, and 700 °C chars. $^{1}H-^{13}C$ long-range dipolar dephasing displayed the same increasing trend of aromatic cluster sizes of wood chars with increasing temperature.

AUTHOR INFORMATION

Corresponding Author

*Telephone: 757-683-6874. Fax: 757-683-4628. E-mail: jmao@odu.edu.

Notes

The authors declare no competing financial interest.

ACKNOWLEDGMENTS

We thank the National Science Foundation (CBET-0853950 and CBET-0853682) for the support of this research.

REFERENCES

(1) Glaser, B.; Haumaier, L.; Guggenberger, G.; Zech, W. The Terra Preta phenomenon: A model for sustainable agriculture in the humid tropics. *Naturwissenschaften* **2001**, *88* (1), 37−41.

(2) Glaser, B.; Lehmann, J.; Zech, W. Ameliorating physical and chemical properties of highly weathered soils in the tropics with charcoal—A review. *Biol. Fertil. Soils* **2002**, *35* (4), 219−230.

(3) Gundale, M. J.; DeLuca, T. H. Temperature and source material influence ecological attributes of Ponderosa pine and Douglas-fir charcoal. *For. Ecol. Manage.* **2006**, *231* (1−3), 86−93.

(4) Sander, M.; Pignatello, J. J. Characterization of charcoal adsorption sites for aromatic compounds: Insights drawn from single-solute and bi-solute competitive experiments. *Environ. Sci. Technol.* **2005**, *39* (6), 1606−1615.

(5) Zhu, D. Q.; Kwon, S.; Pignatello, J. J. Adsorption of single-ring organic compounds to wood charcoals prepared under different thermochemical conditions. *Environ. Sci. Technol.* **2005**, *39* (11), 3990−3998.

(6) Lehmann, J.; Joseph, S. *Biochar for Environmental Management: Science and Technology*; Earthscan: London/ Sterling, VA, 2009.

(7) Demirbas, A. Biomass to charcoal, liquid, and gaseous products via carbonization process. *Energy Sources* **2001**, *23* (6), 579−587.

(8) Demirbas, A. Relationships between carbonization temperature and pyrolysis products from biomass. *Energy Explor. Exploit.* **2004**, *22* (6), 411−419.

(9) Fuwape, J. A. Effects of carbonization temperature on charcoal from some tropical trees. *Bioresour. Technol.* **1996**, *57* (1), 91−94.

(10) Lim, K. O. Quality of cocoa wood charcoal as a function of carbonisation temperature. *Biomass Bioenergy* **1993**, *4* (4), 301−302.

(11) Uchimiya, M.; Wartelle, L. H.; Klasson, K. T.; Fortier, C. A.; Lima, I. M. Influence of pyrolysis temperature on biochar property and function as a heavy metal sorbent in soil. *J. Agric. Food Chem.* **2011**, *59* (6), 2501−2510.

(12) Czimczik, C. I.; Preston, C. M.; Schmidt, M. W. I.; Werner, R. A.; Schulze, E. D. Effects of charring on mass, organic carbon, and stable carbon isotope composition of wood. *Org. Geochem.* **2002**, *33* (11), 1207−1223.

(13) Baldock, J. A.; Smernik, R. J. Chemical composition and bioavailability of thermally, altered *Pinus resinosa* (Red Pine) wood. *Org. Geochem.* **2002**, *33* (9), 1093−1109.

(14) Bardet, M.; Hediger, S.; Gerbaud, G.; Gambarelli, S.; Jacquot, J. F.; Foray, M. F.; Gadelle, A. Investigation with C-13 NMR, EPR, and magnetic susceptibility measurements of char residues obtained by pyrolysis of biomass. *Fuel* **2007**, *86* (12−13), 1966−1976.

(15) Solum, M. S.; Pugmire, R. J.; Jagtoyen, M.; Derbyshire, F. Evolution of carbon structure in chemically activated wood. *Carbon* **1995**, *33* (9), 1247−1254.

(16) Preston, C. M.; Schmidt, M. W. I. Black (pyrogenic) carbon: A synthesis of current knowledge and uncertainties with special consideration of boreal regions. *Biogeosciences* **2006**, *3* (4), 397−420.

(17) McBeath, A. V.; Smernik, R. J. Variation in the degree of aromatic condensation of chars. *Org. Geochem.* **2009**, *40* (12), 1161−1168.

(18) Brewer, C. E.; Schmidt-Rohr, K.; Satrio, J. A.; Brown, R. C. Characterization of biochar from fast pyrolysis and gasification systems. *Environ. Prog. Sustainable Energy* **2009**, *28* (3), 386−396.

(19) McBeath, A. V.; Smernik, R. J.; Schneider, M. P. W.; Schmidt, M. W. I.; Plant, E. L. Determination of the aromaticity and the degree of aromatic condensation of a thermosequence of wood charcoal using NMR. *Org. Geochem.* **2011**, *42* (10), 1194−1202.

(20) Brodowski, S.; Rodionov, A.; Haumaier, L.; Glaser, B.; Amelung, W. Revised black carbon assessment using benzene polycarboxylic acids. *Org. Geochem.* **2005**, *36* (9), 1299−1310.

(21) Glaser, B.; Haumaier, L.; Guggenberger, G.; Zech, W. Black carbon in soils: The use of benzenecarboxylic acids as specific markers. *Org. Geochem.* **1998**, *29* (4), 811−819.

(22) Schneider, M. P. W.; Hilf, M.; Vogt, U. F.; Schmidt, M. W. I. The benzene polycarboxylic acid (BPCA) pattern of wood pyrolyzed between 200 °C and 1000 °C. *Org. Geochem.* **2010**, *41* (10), 1082−1088.

(23) Schneider, M. P. W.; Smittenberg, R. H.; Dittmar, T.; Schmidt, M. W. I. Comparison of gas with liquid chromatography for the determination of benzenepolycarboxylic acids as molecular tracers of black carbon. *Org. Geochem.* **2011**, *42* (3), 275−282.

(24) Hammes, K.; Torn, M. S.; Lapenas, A. G.; Schmidt, M. W. I. Centennial black carbon turnover observed in a Russian steppe soil. *Biogeosciences* **2008**, *5* (5), 1339−1350.

(25) Dittmar, T. The molecular level determination of black carbon in marine dissolved organic matter. *Org. Geochem.* **2008**, *39* (4), 396−407.

(26) Hammes, K.; Schmidt, M. W. I.; Smernik, R. J.; Currie, L. A.; Ball, W. P.; Nguyen, T. H.; Louchouarn, P.; Houel, S.; Gustafsson, O.; Elmquist, M.; Cornelissen, G.; Skjemstad, J. O.; Masiello, C. A.; Song, J.; Peng, P.; Mitra, S.; Dunn, J. C.; Hatcher, P. G.; Hockaday, W. C.; Smith, D. M.; Hartkopf-Froeder, C.; Boehmer, A.; Luer, B.; Huebert,

B. J.; Amelung, W.; Brodowski, S.; Huang, L.; Zhang, W.; Gschwend, P. M.; Flores-Cervantes, D. X.; Largeau, C.; Rouzaud, J. N.; Rumpel, C.; Guggenberger, G.; Kaiser, K.; Rodionov, A.; Gonzalez-Vila, F. J.; Gonzalez-Perez, J. A.; de la Rosa, J. M.; Manning, D. A. C.; Lopez-Capel, E.; Ding, L. Comparison of quantification methods to measure fire-derived (black/elemental) carbon in soils and sediments using reference materials from soil, water, sediment, and the atmosphere. *Global Biogeochem. Cycles* **2007**, *21*, (3).

(27) Ziolkowski, L. A.; Chamberlin, A. R.; Greaves, J.; Druffel, E. R. M. Quantification of black carbon in marine systems using the benzene polycarboxylic acid method: A mechanistic and yield study. *Limnol. Oceanogr.: Methods* **2011**, *9*, 140−149.

(28) Solum, M. S.; Pugmire, R. J.; Grant, D. M. ^{13}C Solid-state NMR of Argonne premium coals. *Energy Fuels* **1989**, *3* (2), 187−193.

(29) Mao, J. D.; Fang, X. W.; Lan, Y. Q.; Schimmelmann, A.; Mastalerz, M.; Xu, L.; Schmidt-Rohr, K. Chemical and nanometer-scale structure of kerogen and its change during thermal maturation investigated by advanced solid-state ^{13}C NMR spectroscopy. *Geochim. Cosmochim. Acta* **2010**, *74* (7), 2110−2127.

(30) Smernik, R. J.; Kookana, R. S.; Skjemstad, J. O. NMR characterization of C-13-benzene sorbed to natural and prepared charcoals. *Environ. Sci. Technol.* **2006**, *40* (6), 1764−1769.

(31) Mao, J. D.; Schmidt-Rohr, K. Recoupled long-range C−H dipolar dephasing in solid-state NMR, and its use for spectral selection of fused aromatic rings. *J. Magn. Reson.* **2003**, *162* (1), 217−227.

(32) Mao, J. D.; Hu, W. G.; Schmidt-Rohr, K.; Davies, G.; Ghabbour, E. A.; Xing, B. S. Quantitative characterization of humic substances by solid-state carbon-13 nuclear magnetic resonance. *Soil Sci. Soc. Am. J.* **2000**, *64* (3), 873−884.

(33) Mao, J. D.; Schmidt-Rohr, K. Accurate quantification of aromaticity and nonprotonated aromatic carbon fraction in natural organic matter by ^{13}C solid-state nuclear magnetic resonance. *Environ. Sci. Technol.* **2004**, *38* (9), 2680−2684.

(34) Dixon, W. T. Spinning-sideband-free and spinning-sideband-only NMR spectra in spinning samples. *J. Chem. Phys.* **1982**, *77* (4), 1800−1809.

(35) Mao, J. D.; Schmidt-Rohr, K. Separation of aromatic carbon ^{13}C NMR signals from di-oxygenated alkyl bands by a chemical-shift-anisotropy filter. *Solid State Nucl. Magn. Reson.* **2004**, *26* (1), 36−45.

(36) Mao, J. D.; Cory, R. M.; McKnight, D. M.; Schmidt-Rohr, K. Characterization of a nitrogen-rich fulvic acid and its precursor algae from solid state NMR. *Org. Geochem.* **2007**, *38* (8), 1277−1292.

(37) Ascough, P. L.; Bird, M. I.; Wormald, P.; Snape, C. E.; Apperley, D. Influence of production variables and starting material on charcoal stable isotopic and molecular characteristics. *Geochim. Cosmochim. Acta* **2008**, *72* (24), 6090−6102.

(38) Mao, J. D.; Holtman, K. M.; Scott, J. T.; Kadla, J. F.; Schmidt-Rohr, K. Differences between lignin in unprocessed wood, milled wood, mutant wood, and extracted lignin detected by ^{13}C solid-state NMR. *J. Agric. Food. Chem.* **2006**, *54* (26), 9677−9686.

(39) Freitas, J. C. C.; Bonagamba, T. J.; Emmerich, F. G. C-13 High-resolution solid-state NMR study of peat carbonization. *Energy Fuels* **1999**, *13* (1), 53−59.

(40) Freitas, J. C. C.; Bonagamba, T. J.; Emmerich, F. G. Investigation of biomass- and polymer-based carbon materials using C-13 high-resolution solid-state NMR. *Carbon* **2001**, *39* (4), 535−545.

(41) Sharma, R. K.; Hajaligol, M. R.; Smith, P. A. M.; Wooten, J. B.; Baliga, V. Characterization of char from pyrolysis of chlorogenic acid. *Energy Fuels* **2000**, *14* (5), 1083−1093.

(42) Pastorova, I.; Botto, R. E.; Arisz, P. W.; Boon, J. J. Cellulose char structure: A combined analytical Py-GC-MS, FTIR, and NMR study. *Carbohydr. Res.* **1994**, *262* (1), 27−47.

(43) David, K.; Pu, Y.; Foston, M.; Muzzy, J.; Ragauskas, A. Cross-polarization/magic angle spinning (CP/MAS) ^{13}C nuclear magnetic resonance (NMR) analysis of chars from alkaline-treated pyrolyzed softwood. *Energy Fuels* **2009**, *23* (1), 498−501.

(44) Sharma, R. K.; Wooten, J. B.; Baliga, V. L.; Hajaligol, M. R. Characterization of chars from biomass-derived materials: Pectin chars. *Fuel* **2001**, *80* (12), 1825−1836.

(45) Sharma, R. K.; Wooten, J. B.; Baliga, V. L.; Lin, X. H.; Chan, W. G.; Hajaligol, M. R. Characterization of chars from pyrolysis of lignin. *Fuel* **2004**, *83* (11−12), 1469−1482.

(46) Link, S.; Arvelakis, S.; Spliethoff, H.; De Waard, P.; Samoson, A. Investigation of biomasses and chars obtained from pyrolysis of different biomasses with solid-state C-13 and Na-23 nuclear magnetic resonance spectroscopy. *Energy Fuels* **2008**, *22* (5), 3523−3530.

(47) Sharma, R. K.; Wooten, J. B.; Baliga, V. L.; Martoglio-Smith, P. A.; Hajaligol, M. R. Characterization of char from the pyrolysis of tobacco. *J. Agric. Food Chem.* **2002**, *50* (4), 771−783.